entropy

MDPI

Article

Entropy Dynamics of Phonon Quantum States Generated by Optical Excitation of a Two-Level System

Thilo Hahn, Daniel Wigger and Tilmann Kuhn *

Institut für Festköpertheorie, Universität Münster, Wilhelm-Klemm-Str. 10 48149 Münster, Germany; t.hahn@wwu.de (T.H.); d.wigger@wwu.de (D.W.)

* Correspondence: tilmann.kuhn@uni-muenster.de

Received: 04 February 2020; Accepted: 27 February 2020; Published: 29 February 2020

Abstract: In quantum physics, two prototypical model systems stand out due to their wide range of applications. These are the two-level system (TLS) and the harmonic oscillator. The former is often an ideal model for confined charge or spin systems and the latter for lattice vibrations, i.e., phonons. Here, we couple these two systems, which leads to numerous fascinating physical phenomena. Practically, we consider different optical excitations and decay scenarios of a TLS, focusing on the generated dynamics of a single phonon mode that couples to the TLS. Special emphasis is placed on the entropy of the different parts of the system, predominantly the phonons. While, without any decay, the entire system is always in a pure state, resulting in a vanishing entropy, the complex interplay between the single parts results in non-vanishing respective entanglement entropies and non-trivial dynamics of them. Taking a decay of the TLS into account leads to a non-vanishing entropy of the full system and additional aspects in its dynamics. We demonstrate that all aspects of the entropy's behavior can be traced back to the purity of the states and are illustrated by phonon Wigner functions in phase space.

Keywords: phonons; two-level system; entropy; Wigner functions; entanglement

1. Introduction

Entropy is one of the most fundamental concepts in physics. According to the second law of thermodynamics, in a closed system, it never decreases, which has far reaching consequences, from the limited efficiency of thermodynamic machines [1] to cosmological implications [2,3]. Under thermal equilibrium conditions, it determines the state of a thermodynamic system: In a closed system, the realized state is the one with maximal entropy; in a system in thermal contact with a heat bath, the realized state results from an interplay between energy and entropy and is governed by the minimum of the free energy [4]. Under nonequilibrium conditions, the second law of thermodynamics prohibits the decrease of the entropy of a closed system; however, this does not hold for the entropy of a subsystem which is interacting with other subsystems or with its surroundings [5,6]. In this case, the study of the dynamics of the entropy of these subsystems provides valuable information on the evolution of the nature of the system's state [7].

From the point of view of information science, entropy is closely related to the imperfect knowledge about a system [8,9]. As such, it plays a key role in all fields related to information processing and communication, and, in particular, in the highly topical fields of quantum information and communication, where the entropy is closely related to phenomena like purity of quantum states, entanglement, and decoherence [10].

In this paper, we study the entropy dynamics in a prototypical model of quantum mechanics and quantum information theory. It consists of two subsystems, a quantum-mechanical two-level system

(i.e., a representation of a qubit) which can be manipulated by an external field (e.g., a light field) and which is coupled to a harmonic oscillator (e.g., a single phonon mode or a nanomechanical oscillator). The generation of specific quantum states of such a harmonic oscillator and the manipulation of these states has recently attracted much interest [11–14]. Prominent examples are coherent states and Schrödinger cat states, i.e., superpositions of coherent states. We analyze the entropy dynamics of the two subsystems after excitation with a short optical pulse or a pair of such pulses. In particular, we compare the case of a unitary evolution in the absence of damping processes, when the coupled system remains in a pure state, with the case of a decaying two-level system resulting in a mixed state also of the combined system. We will show that the analysis of the time-dependent entropy provides interesting insight into the nature of the quantum state of the two subsystems.

2. Theory

We consider a two-level system (TLS) which can be excited and de-excited by a resonant optical field **E**. Additionally, a pure dephasing coupling to a single phonon (ph) mode is taken into account. Thus, the Hamiltonian reads [15]

$$H = \hbar\Omega \left|x\right\rangle \left\langle x\right| - \left[\mathbf{M}\cdot\mathbf{E}(t)\left|x\right\rangle \left\langle g\right| + \mathbf{M}^{*}\cdot\mathbf{E}^{*}(t)\left|g\right\rangle \left\langle x\right|\right] + \hbar\omega_{\mathrm{ph}}\hat{b}^{\dagger}\hat{b} + \hbar g\left(\hat{b}+\hat{b}^{\dagger}\right)\left|x\right\rangle \left\langle x\right| \ . \tag{1}$$

The states $|g\rangle$ and $|x\rangle$ describe ground and excited state of the TLS with an energy splitting of $\hbar\Omega$, respectively. The time dependent optical driving is mediated by the dipole matrix element **M**. Phonons with the discrete energy $\hbar\omega_{\mathrm{ph}}$ are created and annihilated by $\hat{b}^{\dagger}$ and $\hat{b}$, respectively. For simplicity, the coupling constant of the exciton-phonon interaction g is supposed to be real.

Such a TLS system coupled to a single bosonic mode is a prototypical model that can be considered for the description of various solid state systems. For the TLS, one might think of an exciton in a single semiconductor quantum dot [16] or excitations of defects in insulators, like diamond [17] or hexagonal boron nitride [18], while the phonon could be an optical mode [19], a local mode [20], a van Hove singularity [21], or the mechanical excitation of a microresonator [22].

Phonon-induced transitions between the states $|g\rangle$ and $|x\rangle$ of the TLS are negligible because of the strong energy mismatch between the exciton energy, which is of the order of one or a few electronvolts (eV), while phonon energies range from a few micro-electronvolts (μeV) (for micromechanical resonators) up to a few tens of milli-electronvolts (meV) (for optical phonon modes). The linear coupling in the phonon displacement reflects typical electron-phonon interaction mechanisms in solids like deformation potential coupling, piezoelectric coupling, or Fröhlich coupling [23]. Although extensions of this model have been considered that take a quadratic coupling to the phonons into account [24–27], the original independent boson model [28] in Equation (1) is successfully used in different contexts. It reproduces recent linear and nonlinear spectroscopy signals [18,29], Rabi oscillations [30], and rotations [31] in excellent agreement with experiments, to name just a few.

The possible states of the entire system can be separated into the phonons forming product states with the ground state of the TLS and those forming product states with the excited state

$$\left|g\right\rangle \otimes \left|ph_{\mathrm{g}}\right\rangle \qquad \text{and} \qquad \left|x\right\rangle \otimes \left|ph_{\mathrm{x}}\right\rangle \ . \tag{2}$$

From the full density matrix of the system ρ, we can calculate the one of a subsystem by tracing over the respective other, i.e.,

$$\rho_{\mathrm{TLS}} = \mathrm{Tr}_{\mathrm{ph}}(\rho) \qquad \text{and} \qquad \rho_{\mathrm{ph}} = \mathrm{Tr}_{\mathrm{TLS}}(\rho) \ . \tag{3}$$

In the same way as in Reference [32], we model a decay of the excited state with the rate Γ via the Lindblad dissipator

$$\mathcal{D}(\rho) = \Gamma\left[\left|g\right\rangle \left\langle x\right|\rho\left|x\right\rangle \left\langle g\right| - \frac{1}{2}\left\{\left|x\right\rangle \left\langle x\right|,\rho\right\}\right], \tag{4}$$

leading to the master equation for the density matrix:

$$\frac{\mathrm{d}}{\mathrm{d}t}\rho = \frac{1}{i\hbar}[H,\rho] + \mathcal{D}(\rho)\,. \tag{5}$$

We will not take an additional phenomenological pure dephasing of the TLS into account. We will study different regimes of decay rates Γ compared to the characteristic phonon frequency ω_{ph}. On the one hand, when describing, for example, optical phonons with energies in the range of tens of meV the decay time of the TLS is typically much longer than a phonon period, i.e., $\Gamma \ll \omega_{\mathrm{ph}}$ [18]. On the other hand, when considering typical mechanical resonators with phonon energies in the µeV range we have $\Gamma > \omega_{\mathrm{ph}}$ [33].

As we have explained in Reference [32], the entire quantum state and especially the Wigner function of the phonons can be calculated analytically when considering a series of ultrafast laser pulses to drive the TLS. Especially if the pulse duration is much shorter than the phonon period, the pulses can be approximated by delta-functions as

$$\frac{\mathbf{M}\cdot\mathbf{E}(t)}{\hbar} = \sum_j \frac{\theta_j}{2}\exp\left[-i\left(\Omega - \frac{g^2}{\omega_{\mathrm{ph}}}\right)t + i\phi_j\right]\delta(t-t_j)\,. \tag{6}$$

The pulses excite the TLS at times t_j with pulse areas θ_j and phases ϕ_j. By this choice and the introduction of the generating functions

$$Y_\alpha(t) = \left\langle |g\rangle\langle x|\exp(-\alpha^*\hat{b}^\dagger)\exp(\alpha\hat{b})\right\rangle, \tag{7a}$$

$$C_\alpha(t) = \left\langle |x\rangle\langle x|\exp(-\alpha^*\hat{b}^\dagger)\exp(\alpha\hat{b})\right\rangle, \tag{7b}$$

$$F_\alpha(t) = \left\langle \exp(-\alpha^*\hat{b}^\dagger)\exp(\alpha\hat{b})\right\rangle, \tag{7c}$$

with $\langle\hat{A}\rangle = \mathrm{Tr}\left(\rho\hat{A}\right)$ denoting the expectation value of an operator $\hat{A}$, a closed system of partial differential equations for the time-evolution of the generating functions is obtained and all phonon assisted density matrices can be calculated analytically without approximations. Note that F_α contains the entire information on the phonon system, while C_α describes the phonon assisted occupation of the excited state, i.e., the phonons in $|x\rangle\otimes|ph_{\mathrm{x}}\rangle$, and Y_α is the phonon assisted coherence.

Our analysis of the phonon quantum states is based on their Wigner function [34]

$$W(U,\Pi) = \frac{1}{4\pi}\int_{-\infty}^{\infty}\left\langle U+\frac{X}{2}\middle|\rho_{\mathrm{ph}}\middle|U-\frac{X}{2}\right\rangle\exp\left(-\frac{i}{2}X\Pi\right)\mathrm{d}X\,, \tag{8}$$

which is a quasi-probability distribution in the phase space defined by the quadratures $\hat{u}$ and $\hat{\pi}$ and their respective eigenstates

$$\hat{u} = \hat{b}+\hat{b}^\dagger\,, \qquad \hat{\pi} = \frac{1}{i}(\hat{b}-\hat{b}^\dagger)\,, \tag{9a}$$

$$\hat{u}\,|U\rangle = U\,|U\rangle\,, \qquad \hat{\pi}\,|\Pi\rangle = \Pi\,|\Pi\rangle\,. \tag{9b}$$

Due to their definition by the phonon annihilation and creation operators, the quantities U and Π directly correspond to the lattice displacement and momentum, respectively. The generating function F_α, at the same time, is a characteristic function of the Husimi Q function [35]. From this, we can directly calculate the instructive Wigner distribution analytically for a given pulse sequence via [34]:

$$W(U,\Pi,t) = \frac{1}{4\pi^2}\iint_{-\infty}^{\infty}\exp\left(-\frac{|\alpha|^2}{2}\right)F_\alpha(t)\exp\left\{i\left[\mathrm{Re}(\alpha)\Pi + \mathrm{Im}(\alpha)U\right]\right\}\mathrm{d}^2\alpha\,. \tag{10}$$

In the same way, we can isolate the Wigner function W_{x} for the phonons associated with the TLS being in the excited state $|x\rangle$ by choosing C_α instead of F_α in Equation (10). By doing the same, but choosing Y_α, we define W_{p} as the Wigner function of the phonon assisted coherence. In summary, we have

$$F_\alpha \to W\,, \tag{11a}$$
$$C_\alpha \to W_{\mathrm{x}}\,, \tag{11b}$$
$$Y_\alpha \to W_{\mathrm{p}}\,, \tag{11c}$$
$$F_\alpha - C_\alpha \to W - W_{\mathrm{x}} = W_{\mathrm{g}}\,, \tag{11d}$$

where W_{g} is the Wigner function of the phonons associated with the TLS being in the ground state $|g\rangle \otimes |ph_{\mathrm{g}}\rangle$.

Following the original definition by von Neumann [36], we investigate the time-dependent entropy of our coupled quantum system defined by

$$S = -\mathrm{Tr}\big[\rho \ln(\rho)\big]\,. \tag{12}$$

In general, subadditivity states that the entropy of the full system is a lower boundary for the sum of the entropies of the subsystems [37]:

$$S(\rho) \leq S(\rho_{\mathrm{TLS}} \otimes \rho_{\mathrm{ph}}) = S(\rho_{\mathrm{TLS}}) + S(\rho_{\mathrm{ph}})\,. \tag{13}$$

It is important to note that for every pure quantum state ρ_{pure}, the entropy vanishes, i.e.,

$$S_{\mathrm{pure}} = -\mathrm{Tr}\big[\rho_{\mathrm{pure}} \ln(\rho_{\mathrm{pure}})\big] = 0\,, \tag{14}$$

and the entropies of the subsystems coincide if the state of the full system is pure [37]

$$S^{\mathrm{ph}} = S(\rho_{\mathrm{ph}}) = S(\rho_{\mathrm{TLS}})\,. \tag{15}$$

To show this, following Reference [37] for an arbitrary composed system, we decompose the pure state of the entire system $|\psi\rangle$ into an orthonormal basis $|\psi\rangle = \sum_{i,k} C_{ik}|\phi_i\rangle|\chi_k\rangle$ with the coefficient matrix $C = (C_{ik})$. Here, $|\phi_i\rangle$ and $|\chi_k\rangle$ are basis states of the two subsystems, respectively. From the complete density matrix $\rho = (\rho_{ikjl})$, one obtains a reduced density matrix by tracing over the respective other subsystem $\rho_1 = Tr_2(\rho)$:

$$\rho_{ikjl} = \langle\phi_i|\langle\chi_k|\rho|\chi_l\rangle|\phi_j\rangle = C_{ik}C^*_{jl}\,, \tag{16a}$$
$$\Rightarrow \rho_{1,ij} = \langle\phi_i|\rho_1|\phi_j\rangle = \sum_k C_{ik}C^*_{jk} = (CC^\dagger)_{ij}\,. \tag{16b}$$

Analogously the density matrix of the other subsystem is $\rho_2 = C^\dagger C$. Any non-vanishing eigenvalue λ of ρ_1 with the eigenvector $\mathbf{y}$ is then also an eigenvalue of ρ_2 with eigenvector $\mathbf{z} = C^\dagger\mathbf{y}$ because

$$CC^\dagger\mathbf{y} = \lambda\mathbf{y}\,, \tag{17a}$$
$$\Rightarrow C^\dagger C\mathbf{z} = C^\dagger C(C^\dagger\mathbf{y}) = C^\dagger(CC^\dagger)\mathbf{y} = \lambda C^\dagger\mathbf{y} = \lambda\mathbf{z}\,, \tag{17b}$$

and vice versa.

In our particular system, we can choose the TLS's states as the $|\phi_i\rangle \in \{|g\rangle, |x\rangle\}$ and a Fock basis for the phonon system $|\chi_k\rangle \in \{|0\rangle, |1\rangle, \ldots\}$. This means that the coefficient matrix C consists of $2 \times \infty$ elements. The entropy of the TLS, i.e., of its density matrix:

$$CC^\dagger = \rho_{\mathrm{TLS}} = \begin{pmatrix} 1-c & p \\ p^* & c \end{pmatrix} , \qquad \text{with} \quad c = \langle |x\rangle \langle x| \rangle \ , \ p = \langle |g\rangle \langle x| \rangle \ , \tag{18a}$$

can be easily calculated via [37]

$$S(\rho_{\mathrm{TLS}}) = -\lambda_+ \ln(\lambda_+) - \lambda_- \ln(\lambda_-) \, , \tag{18b}$$

where

$$\lambda_\pm = \frac{1}{2} \pm \sqrt{\frac{1}{4} + c^2 - c + |p|^2} = \frac{1}{2} \pm \frac{1}{2}|\mathbf{v}| \tag{18c}$$

are the two eigenvalues of the TLS's density matrix with the Bloch vector $\mathbf{v} = \big(2\mathrm{Re}(p), 2\mathrm{Im}(p), 2c-1\big)$. For a pure state of the full system, according to Equation (17), the phonon density matrix has, despite being a quadratic infinite dimensional matrix, only two non-vanishing eigenvalues $\lambda_\pm$. So, as long as the entire system is in a pure state and we know the entropy of the TLS via Equation (18b), we can derive the entropy of the phonon system by Equation (15).

For an arbitrary, non-pure state of the entire system, the calculation of the entropy in a system with infinite dimensions is far from being trivial. This is the case if, already, the initial state is a statistical mixture, e.g., at non-vanishing temperature or when dephasing leads to a statistical mixture. Therefore, approximations have been discussed and a reasonable version is given by the linear entropy [37]:

$$S_{\mathrm{lin}} = \mathrm{Tr}\big(\rho\big) - \mathrm{Tr}\big(\rho^2\big) = 1 - \mathrm{Tr}\big(\rho^2\big) = 1 - \langle \rho \rangle \ . \tag{19}$$

To get an impression of this approximation, Figure 1a shows the function of the full entropy $-\xi\ln(\xi)$ and the one for the linear entropy $\xi - \xi^2$; similar to the presentation in Reference [37], note that $\mathrm{Tr}(\rho) = 1$. We find that the function of the approximated linear entropy in red is always smaller than the full entropy in blue. Therefore, we expect that the linear entropy under-estimates the full entropy.

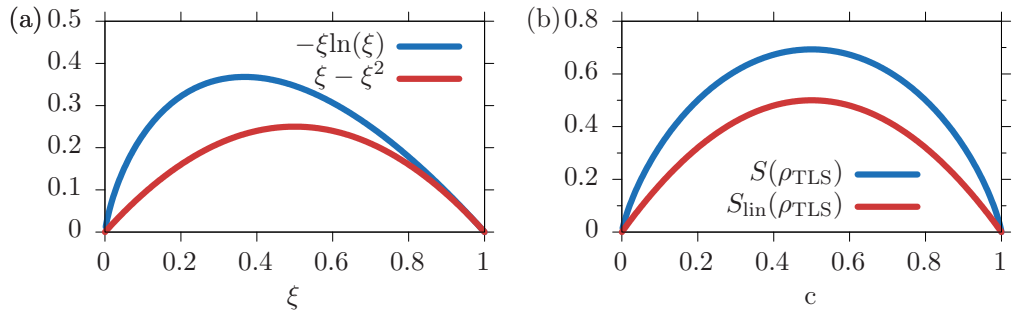

Figure 1. (**a**) Functions for the full entropy in blue and the linear entropy in red. (**b**) Entropies of the two-level system (TLS) with $p = 0$, full entropy in blue and linear entropy in red.

We can directly compare the linear and the full entropy of the isolated TLS from Equation (18b), as shown in Figure 1b. There, the full entropy is plotted in blue and the linear one in red as functions of the excited state occupation c, both for $p = 0$. In the limiting cases of full inversion $c = 1$ and no inversion $c = 0$, the state is pure and both entropies vanish. For all other occupations, the TLS is in a statistical mixture, and the entropy is non-zero, and it is $S_{\mathrm{lin}} \leqslant S$. In the case of an equally distributed mixture, i.e., $c = 0.5$, the entropies are maximal and reach values of $S_{\mathrm{lin}} = 0.5$ and $S = \ln(2) \approx 0.7$.

The biggest advantage of this linear entropy for our study is that it can be directly calculated from the phonons' Wigner functions due to the trace-product rule [38] via

$$S_{\mathrm{lin}}^{\mathrm{ph}} = 1 - 4\pi \iint_{-\infty}^{\infty} W(U,\Pi)^2 \, \mathrm{d}U \, \mathrm{d}\Pi \, . \tag{20}$$

Note that the prefactor 4π depends on the definition of the quadratures U and Π, i.e., the scaling of the phase space.

With the separation into TLS and phonon system, the linear entropy is calculated via

$$S_{\mathrm{lin}} = 1 - \mathrm{Tr}_{\mathrm{ph}}\left[\mathrm{Tr}_{\mathrm{TLS}}\left(\rho^2\right)\right] . \tag{21}$$

For this, we again consider the density matrix of the full system as

$$\rho = (1-c)\,|g\rangle\langle g| \otimes \rho_{\mathrm{ph,g}} + c\,|x\rangle\langle x| \otimes \rho_{\mathrm{ph,x}} + p^*\,|g\rangle\langle x| \otimes \rho_{\mathrm{ph,p}} + p\,|x\rangle\langle g| \otimes \rho^\dagger_{\mathrm{ph,p}} , \tag{22a}$$

$$\Rightarrow \mathrm{Tr}_{\mathrm{TLS}}(\rho^2) = (1-c)^2\rho^2_{\mathrm{ph,g}} + c^2\rho^2_{\mathrm{ph,x}} + |p|^2(\rho_{\mathrm{ph,p}}\rho^\dagger_{\mathrm{ph,p}} + \rho^\dagger_{\mathrm{ph,p}}\rho_{\mathrm{ph,p}}) , \tag{22b}$$

leading to

$$\begin{aligned}\mathrm{Tr}_{\mathrm{TLS}}(\rho) - \mathrm{Tr}_{\mathrm{TLS}}(\rho^2) = {} & (1-c)\rho_{\mathrm{ph,g}} - (1-c)^2\rho_{\mathrm{ph,g}} \\ & + c\rho_{\mathrm{ph,x}} - c^2\rho^2_{\mathrm{ph,x}} \\ & - |p|^2(\rho_{\mathrm{ph,p}}\rho^\dagger_{\mathrm{ph,p}} + \rho^\dagger_{\mathrm{ph,p}}\rho_{\mathrm{ph,p}}) .\end{aligned} \tag{22c}$$

We can now use the separate parts of the Wigner function from Equation (11) to define entropies

$$S^{\mathrm{i}}_{\mathrm{lin}} = \iint_{-\infty}^{\infty}\left[W_{\mathrm{i}}(U,\Pi) - 4\pi W_{\mathrm{i}}(U,\Pi)^2\right]\mathrm{d}U\,\mathrm{d}\Pi , \qquad \text{with } \mathrm{i} \in \{\mathrm{g},\mathrm{x}\} , \tag{22d}$$

$$S^{\mathrm{p}}_{\mathrm{lin}} = -4\pi\iint_{-\infty}^{\infty}|W_{\mathrm{p}}(U,\Pi)|^2\,\mathrm{d}U\,\mathrm{d}\Pi . \tag{22e}$$

Note that the polarization Wigner function W_{p} is a complex quantity. With this and the definitions of the generating functions in Equation (7), we can write the linear entropy in Equation (21) as

$$S_{\mathrm{lin}} = S^{\mathrm{g}}_{\mathrm{lin}} + S^{\mathrm{x}}_{\mathrm{lin}} + 2S^{\mathrm{p}}_{\mathrm{lin}} . \tag{23}$$

To briefly summarize, for pure states of the entire system, i.e., without dephasing or decay of the TLS, we can calculate the full entropy of the phonon state S_{ph} via Equation (15). If the state is not pure, we can at least calculate the linear entropy from the Wigner functions. We can further distinguish between the linear entropy of the full system S_{lin} in Equation (23) and the one of the phonons $S^{\mathrm{ph}}_{\mathrm{lin}}$ in Equation (20).

3. Results and Discussion

3.1. Single Pulse Excitation

We start our study with the most basic situation, where the TLS is excited by a single optical pulse. It is well known from previous works that a single ultrafast excitation in general creates a statistical mixture of coherent states in the phonon system. The excitation of the TLS means for the phonons a shift of the equilibrium position determined by the dimensionless coupling strength $\gamma = g/\omega_{\mathrm{ph}}$. If not stated differently, in the following, we fix this value to $\gamma = 2$ in order to separate the different parts of the Wigner function in phase space, as will be seen later. Although $\gamma = 2$ is a rather large value for quantum dots and optical phonons, the general physics explained in this paper will not depend on this value. Some effects might be strengthened or weakened with a different choice of the coupling strength, as will be highlighted later.

3.1.1. Phonons Generated by a Non-Decaying TLS

In the first step, we neglect the decay of the excited state by choosing $\Gamma = 0$. In this situation, the state of the full system, including the TLS and the phonons, is pure. Therefore, the full and the linearized entropy are zero and Equation (15) holds, meaning that the entropy of the TLS and that of the phonons is the same. Figure 2 recapitulates the phonon dynamics for a pulse area of $\theta = \pi/2$, i.e., an inversion of the TLS of 50% or $c = 0.5$, from Reference [13]. The phonon's Wigner function reads:

$$W(U,\Pi,t) = \frac{1}{4\pi}\left\{ \exp\left[-\frac{1}{2}(U^2+\Pi^2)\right] + \exp\left(-\frac{1}{2}\{U - 2\gamma[1-\cos(\omega_{\mathrm{ph}}t)]\}^2 - \frac{1}{2}[\Pi - 2\gamma\sin(\omega_{\mathrm{ph}}t)]^2\right)\right\}, \tag{24}$$

and its dynamics are shown at five different times in Figure 2a. Before the optical excitation, the phonons are in the vacuum state represented by the Gaussian Wigner function in the center of the phase space. Half of the weight of the phonon's Wigner distribution is brought into the excited state subspace by the optical pulse. This makes them move as a coherent state around the new equilibrium position, which is shifted by 2γ in U-direction. This trajectory is marked as black circle in the figure. The other half of the phonon state remains associated with the ground state of the TLS and, therefore, stays in the vacuum state. The full phonon state after tracing over the TLS states is a statistical mixture of the vacuum state and a coherent state moving around the shifted equilibrium position. After a full phonon period at $t = t_{\mathrm{ph}}$, the Wigner function agrees with the initial situation because the coherent state moves through the origin and overlaps with the vacuum state. The phonon's influence on the properties of the TLS is shown in Figure 2b. While the occupation of the excited state stays constant at $c = 0.5$, the polarization $|p|$ starts at 0.5 directly after the optical excitation at $t = 0$ and drops rapidly to almost zero in the following. This dephasing is inverted towards $t = t_{\mathrm{ph}}$, resulting in a full rephasing to $|p| = 0.5$. While the coherent states separate in phase space, coherence is lost from the TLS, which already shows that the overlap of the different parts of the Wigner function plays an important role for the properties of the entire system.

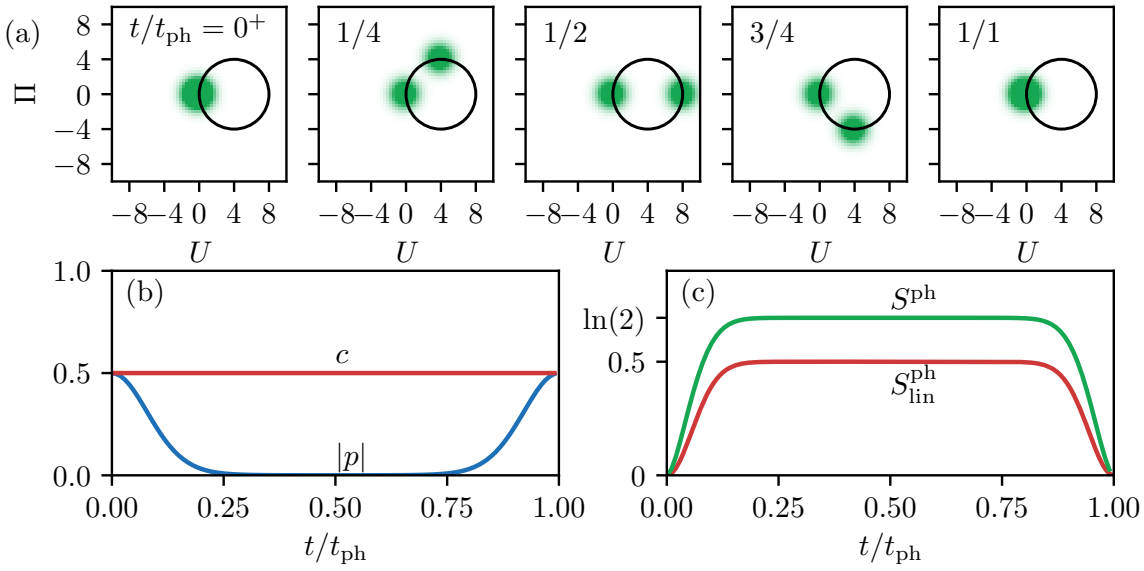

Figure 2. (**a**) Dynamics of the phonon Wigner function after a single pulse excitation of the TLS. (**b**) TLS dynamics with the excited state occupation c in red and the polarization $|p|$ in blue. (**c**) Entropies of the phonon system, S^{ph} in green and $S^{\mathrm{ph}}_{\mathrm{lin}}$ in red.

Finally, in Figure 2c, we show the entropy of the phonons which, as mentioned above, agrees with the entropy of the TLS. As the initial phonon state is pure, both entropies, S^{ph} in green and $S^{\mathrm{ph}}_{\mathrm{lin}}$ in red, start at zero at $t = 0$. While the different parts in phase space separate, the entropy grows to $S^{\mathrm{ph}}_{\mathrm{lin}} \approx 0.5$ because the phonons are in a statistical mixture that must have a non-vanishing entropy. The full entropy follows the same dynamics as the linear one but is always larger, as previously explained, and grows to $S^{\mathrm{ph}} \approx \ln(2) \approx 0.7$. Reaching $t = t_{\mathrm{ph}}$, the entropies drop to zero again. The reason is the recovered overlap of the two parts of the Wigner function. Finally, at $t = t_{\mathrm{ph}}$, the phase space representation cannot be distinguished from the vacuum state. Therefore, the entropy also has to agree with the one of the pure vacuum state being zero.

3.1.2. Phonons Generated by a Decaying TLS

In the previous section, without any decay or additional pure dephasing of the TLS, the quantum state of the entire system remained pure, resulting in a vanishing entropy of the full system. It also allowed us to easily calculate the full entropies for TLS and phonons. In this section, we consider a non-vanishing decay rate of the occupation of the excited state into the ground state, which naturally results in a statistical mixture in the TLS's quantum state that also imprints onto the phonons. Therefore, for the phonons, we can only calculate linear entropies, according to Equation (20). In Reference [32], we explained how the Wigner function evolves during the decay process in the TLS. Therefore, we consider the same optical excitation with a pulse area of $\theta = \pi$, which initially fully inverts the TLS. Without any decay, the Wigner function would read

$$W(U, \Pi, t) = \frac{1}{2\pi} \exp\left(-\frac{1}{2}\{U - 2\gamma[1 - \cos(\omega_{\mathrm{ph}} t)]\}^2 - \frac{1}{2}[\Pi - 2\gamma \sin(\omega_{\mathrm{ph}} t)]^2 \right) , \tag{25}$$

being a single Gaussian moving on a circle around the shifted equilibrium position of the excited state. In Figure 3a, Wigner functions for different decay rates Γ are shown at $t = 10 t_{\mathrm{ph}}$. We find that the phonon state gets smeared out in phase space. For rapid decays on the left, the phonons almost completely stay in the vacuum state and look more or less like a coherent Gaussian distribution. When looking at the corresponding linear entropy dynamics in Figure 3b, in bright red, we see that it only increases slightly after the optical excitation at $t = 0$. When slowing down the decay process, i.e., moving in Figure 3a more to the right, the Wigner function smears out more and more. Accordingly it looks less and less like a coherent state which also leads to increasing entropies in (b) when going from bright to dark colors. Additionally, we find that the final entropy value is reached slower because it follows the decay of the TLS. Especially for the slowest considered decay of $\Gamma = 0.1\omega_{\mathrm{ph}}$, where the full decay takes several phonon periods, the dynamics of the linear phonon entropy develop minima at full phonon periods $t = n t_{\mathrm{ph}}$. These are the times when the Wigner function in Figure 3a starts overlapping itself. This is exemplarily shown in Figure 3c for $t = t_{\mathrm{ph}}$, where the thick Gaussian part is the oscillating coherent state. This is the first time it intersects with the circular distribution that has already decayed into $|g\rangle$. In agreement with the findings in Figure 2, this leads to the temporary reduction of the entropy in Figure 3b.

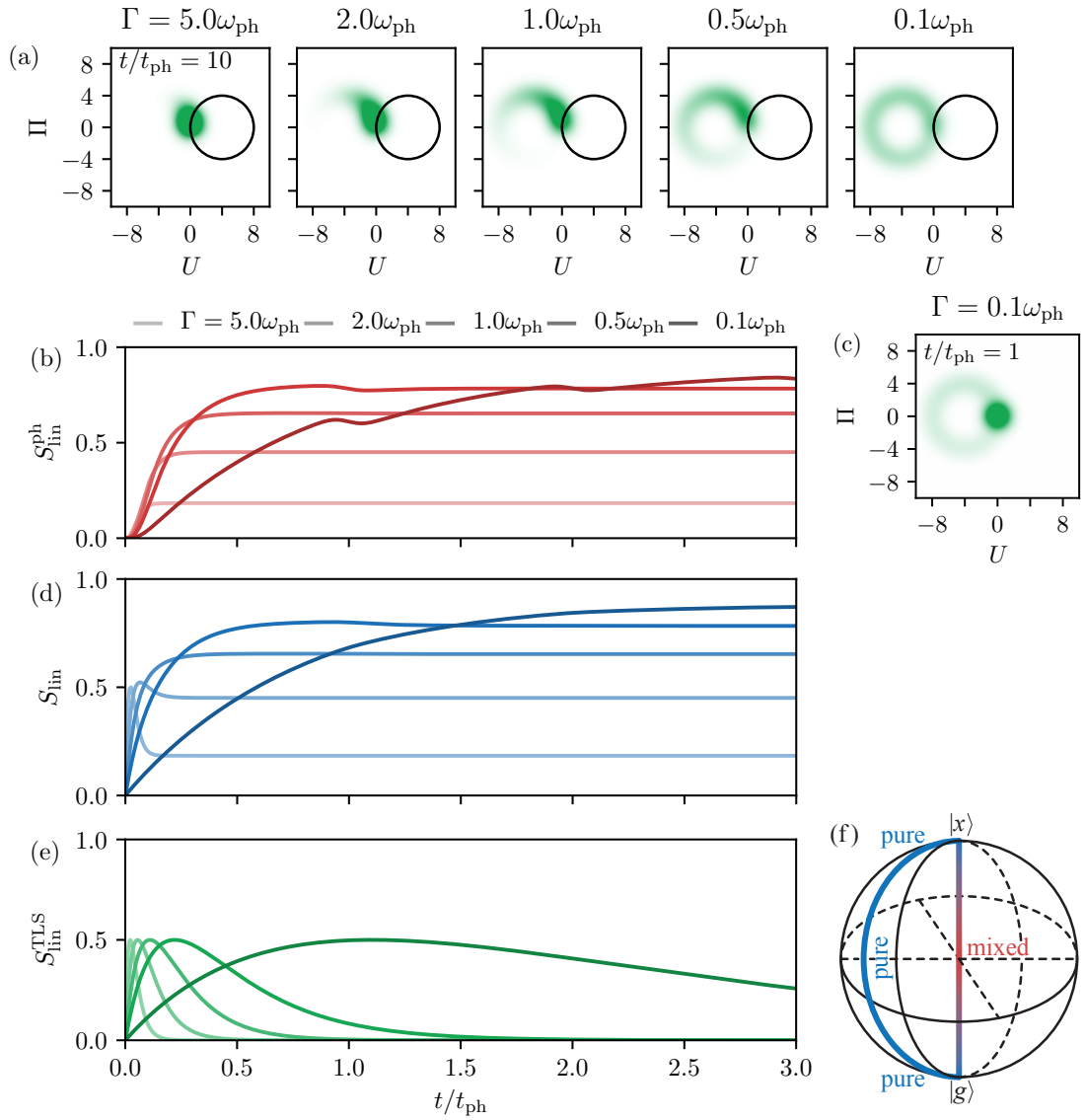

Figure 3. (**a**) Phonon Wigner function after a full decay of the TLS at $t = 10t_{\mathrm{ph}}$ for different decay rates Γ as given in the picture. (**b**) Linear phonon entropy as a function of time after the pulse. The decay rate decreases from bright to dark colors. (**c**) Exemplary Wigner function for a slow decay rate of $\Gamma = 0.1\omega_{\mathrm{ph}}$ at $t = t_{\mathrm{ph}}$. (**d**) Same as (**b**) but for the full linear entropy. (**e**) Same as (**b**) but for the linear entropy of the TLS. (**f**) Bloch sphere of the TLS to illustrate the purity of different states; blue shows pure and red mixed states.

Comparing the linear entropy of the phonon system in Figure 3b with the linear entropy of the entire system S_{lin} in (d), we basically find the same overall behavior. The dynamics start at zero, the final values increase for smaller decay constants, and the final values are reached later. However, both for small and large Γ, we find qualitative differences. Starting with small Γ in dark blue, especially for $\Gamma = 0.1\omega_{\mathrm{ph}}$, the curve constantly grows without developing any minima. This shows that the reduction of phonon entropy due to the overlapping Wigner functions does not attain to the full entropy. The reason for this is that the reduction of the phonon entropy due to overlapping parts of the Wigner function only happens because the state information of the TLS has been traced out. Taking the entire coupled system into account, the overlapping phonon parts belong to different states of the TLS and can therefore be told apart. Therefore, the phonons do not lead to a depression of the full linear entropy. Conversely, for large decay rates, in bright blue, especially $\Gamma = 5\omega_{\mathrm{ph}}$, we find that, on a short timescale around $t = 0.1t_{\mathrm{ph}}$, a pronounced maximum appears in S_{lin}. This effect is not

found in the phonon part in Figure 3b and therefore stems from the TLS contribution. To understand this, in Figure 3e, we plot the linear entropy of the TLS as green lines. The bright and dark colors agree with the ones in Figure 3b,d. In addition, we consider the schematic Bloch vector representation of the TLS state from Equation (18c) in Figure 3f. The z direction of the Bloch sphere depicts the occupation of the states, where the south pole is a pure ground state $|g\rangle$ and the north pole a pure excited state $|x\rangle$. Between these points, all Bloch vectors that are on the surface of the sphere (blue line) are superpositions $|\chi\rangle = N(\alpha\,|g\rangle + \beta\,|x\rangle)$ and are therefore pure. In the other extreme case of the line directly connecting north and south pole (red), the system is in a statistical mixture of $|g\rangle$ and $|x\rangle$. In the center of the Bloch sphere, the TLS is in both states with equal probability, resulting in the lowest purity. For the entropy of the TLS in Figure 3e, this means that, directly after the excitation into the excited state and after the full decay, the entropy is zero. In between, the system evolved through a statistical mixture, which has a non-vanishing entropy. The linear entropy reaches maxima with $S_{\mathrm{lin}}^{\mathrm{TLS}} = 0.5$, in agreement with the result in Figure 1b.

If we want to determine the final linear entropy $S_{\mathrm{lin}}^{\mathrm{ph},\infty} = S_{\mathrm{lin}}^{\mathrm{ph}}(t \to \infty)$ of the phonon state after the TLS is fully decayed into the ground state, we can investigate the dynamics in phase space. Note that the final entropy is only carried by the phonon part because the TLS is in the pure ground state. As schematically shown in Figure 4a, the movement of the coherent state on the circle in the excited state subspace and the accompanied decay into the ground state leads to a distribution that can be seen as a continuous distribution of coherent states with decreasing amplitude. We can parametrize the circular motion of the Wigner function including the decay of the amplitude by

$$W_{\infty}(U,\Pi) = \Gamma \int_0^{\infty} \exp(-\Gamma t) W_{(U_0(t),\Pi_0(t))}\,\mathrm{d}t\,, \tag{26}$$

where $W_{(U_0(t),\Pi_0(t))}$ is a Gaussian centered around $(U,\Pi) = (U_0(t),\Pi_0(t))$. With the circular trajectory in Equation (25), we have to consider

$$U_0(t) = 2\gamma[1-\cos(\omega_{\mathrm{ph}}t)] \qquad \text{and} \qquad \Pi_0(t) = 2\gamma\sin(\omega_{\mathrm{ph}}t)\,. \tag{27}$$

Note that, to retrieve the Wigner distribution in the ground state in Figure 3a, one has to mirror the schematic in Figure 4a. However, the final linear entropy remains unaffected because it only depends on the general shape of the distribution. With this, the final linear entropy reads

$$\begin{aligned} S_{\mathrm{lin}}^{\mathrm{ph},\infty} &= 1 - 4\pi \iint_{-\infty}^{\infty} W_{\infty}^2(U,\Pi)\,\mathrm{d}U\mathrm{d}\Pi \\ &= 1 - 4\pi\Gamma^2 \iint_{-\infty}^{\infty} \iint_{0}^{\infty} \exp\left[-\Gamma(t+t')\right] W_{(U_0(t),\Pi_0(t))} W_{(U_0(t'),\Pi_0(t'))}\,\mathrm{d}t\mathrm{d}t'\,\mathrm{d}U\mathrm{d}\Pi\,. \end{aligned} \tag{28}$$

The integral over U and Π describes the overlap of two coherent states in phase space. In general, two coherent states with a phase space distance of a have an overlap of [34]

$$4\pi \iint_{-\infty}^{\infty} W_{(0,0)} W_{(a,0)}(U,\Pi)\,\mathrm{d}U\mathrm{d}\Pi = \exp\left[-\frac{a^2}{4}\right]\,. \tag{29}$$

Therefore, the entropy becomes

$$S_{\mathrm{lin}}^{\mathrm{ph},\infty} = 1 - \Gamma^2 \iint_{0}^{\infty} \exp\left[-\Gamma(t+t')\right] \exp\left(-\left\{2\gamma\sin\left[\frac{1}{2}\omega_{\mathrm{ph}}(t-t')\right]\right\}^2\right) \mathrm{d}t\mathrm{d}t'\,. \tag{30}$$

The sine function in the exponent can be approximated by a linear function for small frequencies or short times. Note that, although the integration is carried out up to $t = \infty$, the exponential decay with Γ effectively limits the integrated time interval. Therefore, we expect this approximation to work well for sufficiently large Γ. For the motion of the Wigner function, this corresponds to a linear movement in phase space, as schematically shown in Figure 4b. The corresponding linear entropy can then be calculated to

$$\begin{aligned} S_{\mathrm{lin}}^{\mathrm{ph},\infty} &\approx 1 - \Gamma^2 \int_0^\infty\!\!\int \exp\left[-\Gamma(t+t')\right] \exp\left\{-[\gamma\omega_{\mathrm{ph}}(t-t')]^2\right\} \mathrm{d}t\mathrm{d}t' \\ &= 1 - \frac{\sqrt{\pi}\,\Gamma}{2\gamma\omega_{\mathrm{ph}}} \exp\left[\left(\frac{\Gamma}{2\gamma\omega_{\mathrm{ph}}}\right)^2\right] \mathrm{erfc}\left(\frac{\Gamma}{2\gamma\omega_{\mathrm{ph}}}\right), \end{aligned} \tag{31}$$

where $\mathrm{erfc}(x) = 1 - \mathrm{erf}(x)$ and $\mathrm{erf}(x)$ are the error function.

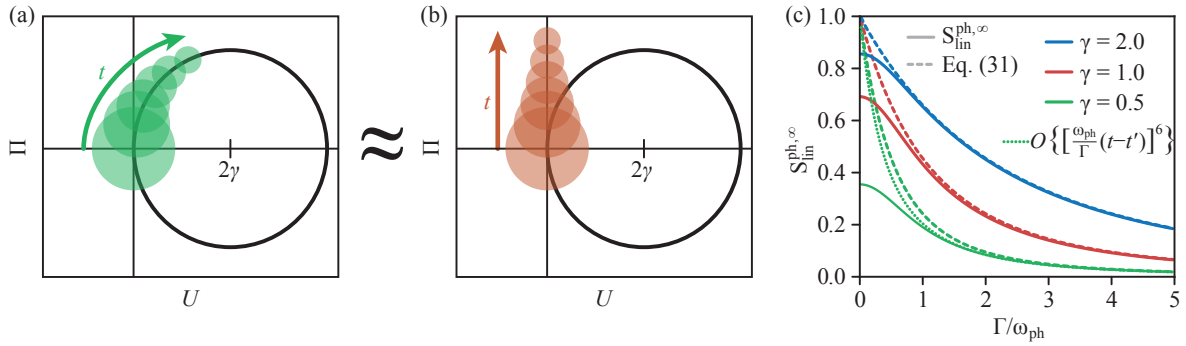

Figure 4. Final value of the entropy after the full decay of the TLS. (**a**) Schematic of the phase space dynamics of the Wigner function during the decay. (**b**) Approximated dynamics as a straight line. (**c**) Final linear entropy $S_{\mathrm{lin}}^{\mathrm{ph},\infty}$ as a function of the decay rate Γ, full simulation in solid and approximation from Equation (31) in dashed lines. Different coupling strengths are shown in blue, red, and green. The dotted green line shows the entropy for an expansion of the squared sine-function up to the sixth order.

The results for the final entropy $S_{\mathrm{lin}}^{\mathrm{ph},\infty}$ are shown in Figure 4c as a function of the decay rate Γ, where the full calculations according to the dynamics are shown as solid lines and the approximations from Equation (31) are the dashed lines. We show the three different coupling strengths $\gamma = 2$ (blue), $\gamma = 1$ (red), and $\gamma = 0.5$ (green). Comparing the different coupling strengths, we find that a stronger coupling leads to a larger final entropy because the Wigner function gets distributed over a larger area of phase space. As explained before, the approximation in Equation (31) works very good for large Γ, but we also see that the approximation works over a larger Γ range if the coupling strength is larger. The reason for this is that, for larger γ, the circle of the Wigner function's trajectory is larger, meaning that its curvature can be better approximated by a linear motion. For the smallest considered coupling strength $\gamma = 0.5$, in green, we additionally show the dotted line that stems from an approximation of the squared sine function up to the sixth order, which is the next non-divergent contribution in Equation (30). This curve is obviously a better approximation of the full calculation, in particular, in the range $1 \lesssim \Gamma/\omega_{\mathrm{ph}} \lesssim 2$. However, in agreement with all dashed lines, it reaches $S_{\mathrm{lin}}^{\mathrm{ph},\infty} = 1$ for $\Gamma = 0$, while all full linear entropies go to smaller values. This shows that any approximation of the sine function will not give accurate results for very small decay rates. In fact, it turns out that, for any finite (converging) order of the expansion of the squared sine function in Equation (30), $S_{\mathrm{ph}}^{\mathrm{lin},\infty} = 1$ is reached in the limit $\Gamma \to 0$. This can be understood by realizing that, for any finite order in the expansion of the trigonometric functions in Equation (27), the trajectory tends to infinity for $t \to \infty$, thus leading to a delocalized Wigner function. On the other hand, the correct

Wigner function in this limit is the doughnut-shaped function similar to the rightmost function in Figure 3a, for which the linear entropy can be calculated analytically, yielding

$$S_{\mathrm{ph}}^{\mathrm{lin},\infty} = 1 - e^{-2\gamma^2} I_0\left(2\gamma^2\right) , \tag{32}$$

with the modified Bessel function of first kind and zeroth order I_0, in perfect agreement with the numerical results given in Figure 4c.

3.2. Two Pulse Excitation

The phonon quantum state gets more involved when a two-pulse excitation is considered. As extensively studied in Reference [13,32], an excitation with two pulses having pulse areas of $\theta_1 = \theta_2 = \pi/2$ and a delay of $t_2 - t_1 = t_{\mathrm{ph}}/2$ leads to the generation of two Schrödinger cat states, each in one TLS subspace. A Schrödinger cat state is a coherent superposition of two coherent states, i.e., of the most classical states of a harmonic oscillator, and, as such, it is of high interest in all areas of quantum optics [39–41] and, more recently, also phononics [11].

3.2.1. Phonons Generated by a Non-Decaying TLS

We assume the same excitation scheme as just described and again disregard any decays of the TLS. The dynamics of the Wigner function are exemplarily shown in Figure 5a. Immediately before the second laser pulse reaches the TLS, the phonons are in the statistical mixture previously shown in Figure 2a. The second pulse creates a second coherent state in the excited state subspace of the TLS, but it also makes half of the coherent state in $|x\rangle$ go back to the ground state. Therefore, we end up with two coherent states in both subspaces, $|g\rangle$ and $|x\rangle$. As nicely seen in Figure 5a, the corresponding Wigner function shows two of the classic dumbbell structures of the cat state, two Gaussians and a striped structure of alternating positive (green) and negative (orange) values between them. These stripes indicate the interference between the two coherent states. The Wigner function in the ground state rotates around the origin, and the one in the excited state around the shifted equilibrium at $(U, \Pi) = (2\gamma, 0) = (4, 0)$ is marked by the black circle.

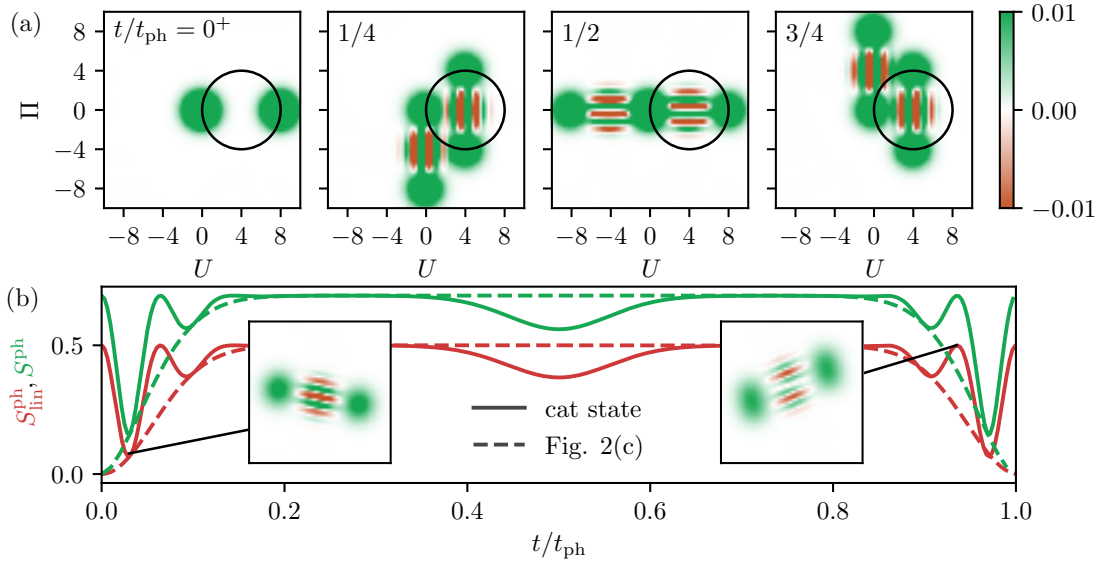

Figure 5. Two pulse excitation without decay. (**a**) Snapshots of the Wigner function after the second pulse. (**b**) Entropy dynamics after the second pulse, solid lines are the entropies of the cat states, dashed lines the statistical mixture from Figure 2c. The full phonon entropy is green and the linear one red.

The entropies of the phonon state are shown in Figure 5b as solid lines. The linear entropy in red starts at $S_{\mathrm{lin}} = 0.5$ in agreement with the entropy in Figure 2d at $t = t_{\mathrm{ph}}/2$ because at this time the second pulse excites the TLS. In contrast to the behavior after the first pulse, here, the entropy drops very rapidly and forms a sharp minimum after the second pulse. In total, the entropy performs two oscillations before remaining constant at the initial value. The same dynamics repeat themselves in an inverted form before reaching a full period. Another striking feature is a smaller depression around $t = t_{\mathrm{ph}}/2$. Overall, we find that, by the second pulse, the entropy of the phonon is temporarily reduced but never increased. The maximum entropy is here the one of a statistical mixture of two fully separated coherent states (see Figure 2), which is obviously the same for a statistical mixture of two cat states that are fully separated. This is the case during the times around $t/t_{\mathrm{ph}} = 1/4$ and $t/t_{\mathrm{ph}} = 3/4$ (see Figure 5a). Next, we discuss the reduced entropy around half a period in Figure 5b. Looking at the corresponding Wigner function in Figure 5a, we find that this is the time when one of the coherent states in the excited state system (moving on the circle) overlaps with the vacuum state (staying at the origin). This is the same effect as discussed in the previous sections, where the entropy shrank when the phonon states were overlapping in phase space. Finally, we have to understand the strong reductions of the entropy for times around full periods. To do so, we examine the two insets in Figure 5b that show snapshots of the Wigner function at the marked times, i.e., where the entropy is minimal and maximal. The left one at the minimum depicts a time where each of the two Gaussians starts to split into two, which cannot yet be resolved in the figure because their overlap is still too large. However, the interference terms between them also move apart. At $t = 0$, their negative and positive values are distributed in such a way that they exactly compensate each other (see $t = 0^+$ in Figure 5a). But, in the left inset, we see that at this time negative and positive values add up, respectively, making for an accurate alternating pattern. Comparing this structure of the Wigner function with one of the cat states in Figure 5a shows a strong resemblance. So, the reason for the strong decrease of the entropy is that, at these times, the Wigner function can only hardly be distinguished from a single Schrödinger cat state, which is a pure state. Likewise, we can analyze the Wigner function at a maximum of the entropy oscillation in the right inset. In addition, here, the Gaussians have a large overlap, but the stripes of the interferences are aligned in such a way that the line in the center has vanishing values. This strongly disagrees with the natural structure of a cat state interference and makes it easily distinguishable from that pure cat state. The full phonon entropy S^{ph} is shown as a green solid line. It follows the same dynamics as the linear one but is just scaled to larger values, as discussed before. Finally, let us remark on the additionally plotted dashed lines, which are the respective entropy curves from Figure 2c. They exactly form envelopes for the oscillations and therefore demonstrate that the oscillating dynamics are again a result of the separation process of the different Wigner functions in phase space.

The relative phase of the two laser pulses changes the phase in the cat states, i.e., the phase of the striped structure of the Wigner function. As long as the different parts of the phonon state are separated in phase space, the phase has no influence on the phonon entropy. The other crucial parameter of the phonon system is the coupling strength γ that determines the distance of the coherent states and the number of stripes in the interference term, as exemplarily shown in Figure 6a,b. The influence of an increased coupling strength is presented in Figure 6c, where the linear phonon entropy $S^{\mathrm{ph}}_{\mathrm{lin}}$ is plotted in the same way as in Figure 5b but only for times up to $t/t_{\mathrm{ph}} = 0.25$. The red curve shows $\gamma = 2$ from Figure 5b as a reference. Looking at the larger coupling in bright red ($\gamma = 4$) and a smaller coupling in dark red ($\gamma = 1.5$), we clearly see that the oscillation of the entropy gets faster when γ grows and more minima evolve. The reason is that the interference terms consist of more stripes that run through each other. At the same time, the envelope gets shorter for a larger γ, which can be traced back to the larger spread of the Wigner function in phase space. While the sizes of the interference terms and the Gaussians stay the same, as shown in Figure 6a,b, the radius of the trajectory increases. Because the angular frequency of the motion remains the same, the two interferences separate in a shorter time, and this time determines the envelope of the entropy in Figure 6c.

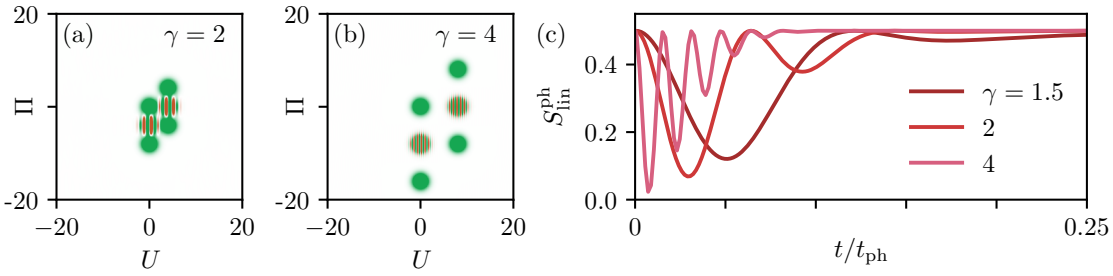

Figure 6. (**a**,**b**) Exemplary Wigner functions at $t = t_{\mathrm{ph}}/4$ for $\gamma = 2$ in (**a**) (same as in Figure 5a) and $\gamma = 4$ in (**b**). (**c**) Linear phonon entropy $S_{\mathrm{lin}}^{\mathrm{ph}}$ as a function of time after a two-pulse excitation as in Figure 5b. The coupling strength γ increases from dark to bright red.

3.3. Phonon Cat State Entropy Dynamics in a Decaying TLS

Next, we increase the complexity of the considered phonon state by analyzing the influence of the decay of the TLS on the entropy dynamics of cat states. For reasons of clarity, we consider a single Schrödinger cat state entirely in the excited state $|x\rangle \otimes |\mathrm{cat}\rangle$ as initial state without any optical excitation and account for a decay of the TLS into its ground state. Although this state cannot directly be prepared by optical pulses, in Reference [32] it is explained how it is constructed mathematically as initial state for the simulated decay dynamics. Some snapshots of the corresponding Wigner function dynamics are shown in Figure 7a for a small decay rate of $\Gamma = 0.1\omega_{\mathrm{ph}}$. As analyzed in Reference [32], the combined rotation and shift of the phonon equilibrium position due to the decay of the TLS finally leads to a Wigner function in the shape of an eight. Note that, for a slow decay where the coherent parts lead to a homogeneously distributed eight-shape, two interference terms transferred into the ground state at $t/t_{\mathrm{ph}} = (2n+1)/4$ survive the decay process.

The corresponding linear entropies are depicted in Figure 7b, where the blue curves show the linear entropy of the full system S_{lin} and the red ones the linear entropy of the phonons $S_{\mathrm{lin}}^{\mathrm{ph}}$. The decay rate increases from dark to bright colors. We find the same dependency on the decay rate as for a single coherent state in Figure 3b,d, the final entropy increases for a slower decay. In addition, the behavior for very fast decays, e.g., $\Gamma = 5\omega_{\mathrm{ph}}$, is approximately the same as in Figure 3. The entropy of the full system (light blue) forms a sharp peak due to the evolution of the TLS through a statistical mixture, while the phonon part (light red) basically just rises before reaching the stationary value. The dynamics get more involved and new features appear for slow decays, e.g., for $\Gamma = 0.05\omega_{\mathrm{ph}}$. Here, the full entropy in dark blue continuously increases to the stationary value at the end of the decay process, while the phonon contribution in dark red is always slightly smaller and shows additional dynamics developing multiple minima and maxima within each phonon period. While the dynamics are rather irregular on shorter times $t < 3t_{\mathrm{ph}}$, it becomes more periodic for longer periods of time.

To understand the origin of these dynamics in the phonon system, we take a closer look at the different parts of the Wigner function. According to Reference [13], the Wigner function of a cat state can be separated into

$$W = W_{\mathrm{coh}} + W_{\mathrm{int}}\,, \tag{33}$$

where W_{coh} describes the two coherent states that have been studied previously, and W_{int} is the interference showing up as striped structure in phase space. Under the assumption that the phonon coupling strength, γ is large enough such that the different parts of the Wigner function do not significantly overlap in phase space; the linear entropy can also be separated into two contributions, $S_{\mathrm{lin}}^{\mathrm{coh}}$ and $S_{\mathrm{lin}}^{\mathrm{int}}$, calculated from the respective contributions of the Wigner function, and we obtain

$$S_{\mathrm{lin}}^{\mathrm{ph}} \approx S_{\mathrm{lin}}^{\mathrm{coh}} + S_{\mathrm{lin}}^{\mathrm{int}}\,. \tag{34}$$

In Figure 7c, we show the different entropies for a short time window $4 \leqslant t/t_{\mathrm{ph}} \leqslant 5$. This already clarifies the picture a bit. First of all, we find that $S_{\mathrm{lin}}^{\mathrm{coh}}$ (green) and $S_{\mathrm{lin}}^{\mathrm{int}}$ (blue) are approximately of the same size and the sum of the two parts, shown in dashed blue, agrees perfectly with the full linear phonon entropy (red line). The coherent part $S_{\mathrm{lin}}^{\mathrm{coh}}$ has reduced values at times $t/t_{\mathrm{ph}} = n/2$, and $S_{\mathrm{lin}}^{\mathrm{int}}$ develops minima exactly between those times, i.e., at $t/t_{\mathrm{ph}} = (2n+1)/4$. Because the shapes of the minima in the two contributions are not the same, the sum appears quite involved.

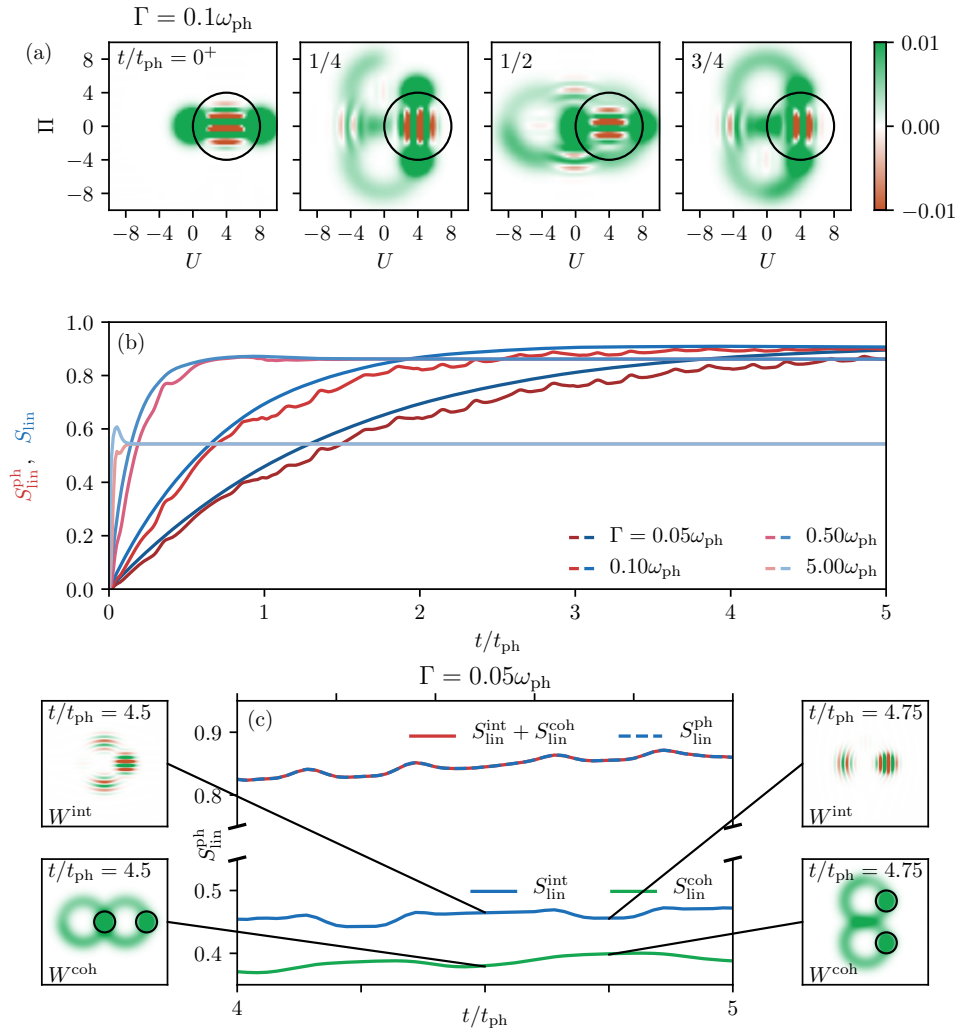

Figure 7. (**a**) Snapshots of the Wigner function during the decay into the ground state for a decay rate of $\Gamma = 0.1\omega_{\mathrm{ph}}$. (**b**) Linear phonon entropies in red and full linear entropies in blue as functions of time for different decay rates. Γ increases from bright to dark colors. (**c**) Zoom-in on one phonon period for $\Gamma = 0.05\omega_{\mathrm{ph}}$. The coherent contribution $S_{\mathrm{lin}}^{\mathrm{coh}}$ is green, the one from the interference $S_{\mathrm{lin}}^{\mathrm{int}}$ is blue and their sum dashed blue. Next to (**c**) are exemplary Wigner functions of the coherent part (bottom) and the interference (top) for the respective minima marked by black lines.

After identifying the different dynamics, we have to understand their origin. Therefore, next to Figure 7c, we plot the Wigner functions W_{coh} and W_{int} for the respective minima, as marked by the black lines. Starting with the coherent part at the bottom, we recognize that the situation is equivalent to the one in Figure 3b,c. The entropy is always reduced when the rotating Wigner function of the coherent states in the excited state subspace (marked by black circles) overlaps with parts of the Wigner function in the ground state subspace. In the right example, at $t = 4.75t_{\mathrm{ph}}$, the two Gaussians are clearly separated from the decayed part in the ground state. In the left one, at $t = 4.5t_{\mathrm{ph}}$, one of the coherent states overlaps with the touching point of the two circles that are in the ground state $|g\rangle$.

Because we start with two coherent states in $|x\rangle$, the periodicity of the minima is half the phonon period. Moving on to the Wigner function of the interference contribution at the top, we only see the expected striped patterns. The times where $S_{\mathrm{lin}}^{\mathrm{int}}$ is reduced agree with the times $t/t_{\mathrm{ph}} = (2n+1)/4$, where the interference terms that survive the decay process and remain also after the full decay are transferred into the ground state system (see discussion in Reference [32]). As seen in the depicted Wigner function on the right, at these times (e.g., $t = 4.75t_{\mathrm{ph}}$) in Figure 7c, one of the interference terms that were already transferred into $|g\rangle$ perfectly overlaps with the single interference that is still in the excited state, resulting in the two separated structures in phase space. For all other times, three contributions appear, two in $|g\rangle$ and one in $|x\rangle$, as exemplarily shown on the left for $t = 4.5t_{\mathrm{ph}}$. Thus, the fundamental reason for the reduction of the entropy is that a mixture of two cat states is more pure than a mixture of three. The perfectly overlapping interferences on the right make the corresponding Wigner function look more like a mixture of two states than of three.

3.3.1. Phonons Generated by a Decaying TLS

To conclude the discussion, we now take a look at the two pulse excitation discussed in Section 3.2.1 and consider a non-vanishing decay rate of the TLS. In Reference [32], it was shown that the final phonon state is in good agreement with the eight-shaped Wigner function of the decayed single cat state previously analyzed. However, now the phonon generation leads to a statistical mixture of two cat states that are additionally smeared out in phase space. This is exemplarily shown by the Wigner functions in Figure 8a. Although the quantum state of the system is more involved, the linear entropy of the phonons depicted as red line in Figure 8b evolves in a well-structured manner. Especially after the excitation with the second pulse, marked by the dashed black line, the dynamics resemble the ones in Figure 5b with an additional increase of the curve according to the decay process. We find the same broad depressions for half periods and stronger oscillating ones for full periods. The small additional entropy reductions discussed in Figure 7 are also found here, as shown by the zoom-in in Figure 5c. However, compared to the effects of the two overlapping cat states, as previously mentioned, they almost disappear. The linear entropy of the full system shown as a blue line in Figure 5b is always smaller than the phonon part and grows smoothly. This is in agreement with the situation without any decay, where the entropy of the full system was always zero while the phonon part was non-vanishing.

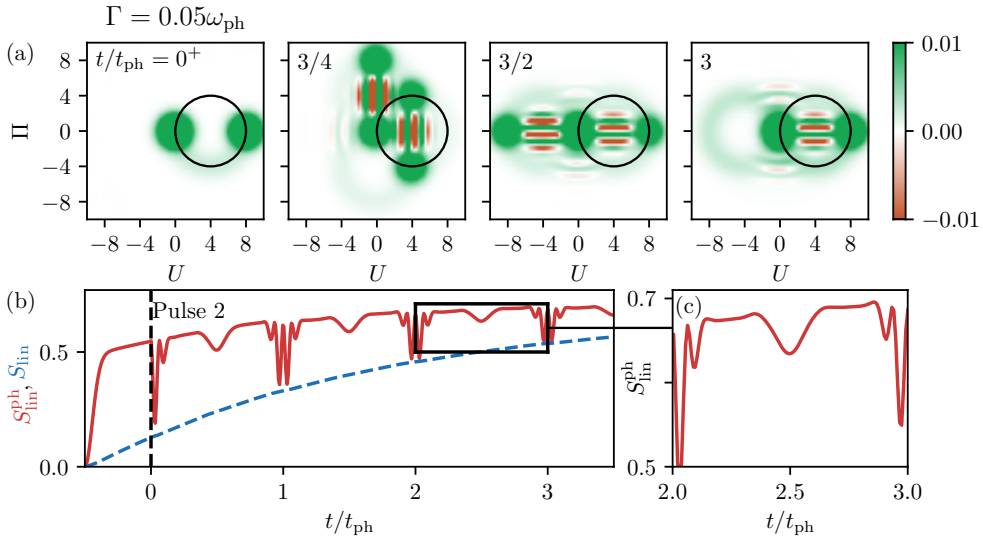

Figure 8. (**a**) Snapshots of the Wigner function's dynamics after the second pulse for $\Gamma = 0.05\omega_{\mathrm{ph}}$. (**b**) Dynamics of the linear phonon entropy in red and the linear entropy of the full system in blue. (**c**) Zoom-in on the marked short time window from (**b**).

4. Conclusions

In summary, we analyzed the entropy dynamics of a single phonon mode coupled to an optically-driven TLS. We presented a theoretical framework that allowed us to calculate entropies of the different parts of the system when the quantum state of the entire system is pure and linear entropies when it is not pure. Additionally, the concept of Wigner functions for the representation of phonon quantum states was used. We started our discussion with the most basic optical excitation, i.e., a single ultrafast pulse, that generated a mixture of two coherent states in the phonon system and assumed a non-decaying TLS. From this, we further increased the complexity of the generated phonon state by including non-vanishing decay rates and two-pulse excitations of the TLS. This led to Wigner functions that smeared out in phase space and the generation of Schrödinger cat states, respectively. While the decay of the TLS, in general, led to an increase of the system's entropy, the complex dynamics of the phonon states resulted in temporally significant reductions of the phonon entropy. All these effects could be traced back to the purity of the quantum states and the entanglement between phonons and TLS. This extensive study on the phonon's entropy led to a thorough understanding of the fundamental interplay between the dynamics of the two separate parts and their combined influence on the quantum state purity.

Author Contributions: conceptualization, T.H., D.W. and T.K.; methodology, T.H.; software, T.H.; validation, T.H., D.W. and T.K.; formal analysis, T.H.; investigation, T.H.; data curation, T.H.; writing–original draft preparation, D.W.; writing–review and editing, T.H., D.W. and T.K.; visualization, T.H. and D.W.; supervision, D.W. and T.K.; project administration, T.K. All authors have read and agreed to the published version of the manuscript.

Funding: This research received no external funding.

Conflicts of Interest: The authors declare no conflict of interest.

References

1. Kondepudi, D.; Prigogine, I. *Modern Thermodynamics: From Heat Engines to Dissipative Structures*; John Wiley & Sons: Berlin, Germany, 2014.
2. Gunzig, E.; Geheniau, J.; Prigogine, I. Entropy and cosmology. *Nature* **1987**, *330*, 621–624. [CrossRef]
3. la Cruz-Dombriz, D.; Sáez-Gómez, D. Black holes, cosmological solutions, future singularities, and their thermodynamical properties in modified gravity theories. *Entropy* **2012**, *14*, 1717–1770. [CrossRef]
4. Toda, M.; Kubo, R.; Saitō, N. *Equilibrium Statistical Mechanics*; Springer: Berlin, Germany, 1992; Volume 1.
5. Kubo, R.; Toda, M.; Hashitsume, N. *Statistical Physics II: Nonequilibrium Statistical Mechanics*; Springer: Berlin, Germany, 2012; Volume 31,
6. Breuer, H.P.; Petruccione, F. *The Theory of Open Quantum Systems*; Oxford University Press: Oxford, UK, 2002.
7. Eisert, J.; Cramer, M.; Plenio, M.B. Colloquium: Area laws for the entanglement entropy. *Rev. Mod. Phys.* **2010**, *82*, 277. [CrossRef]
8. Shannon, C.E. A mathematical theory of communication. *Bell Labs Tech. J.* **1948**, *27*, 379–423. [CrossRef]
9. Liang, J.; Shi, Z.; Li, D.; Wierman, M.J. Information entropy, rough entropy and knowledge granulation in incomplete information systems. *Int. J. Gen. Syst.* **2006**, *35*, 641–654. [CrossRef]
10. Nielsen, M.A.; Chuang, I. *Quantum Computation and Quantum Information*; American Association of Physics Teachers: College Park, MD, USA, 2002.
11. Hofheinz, M.; Wang, H.; Ansmann, M.; Bialczak, R.C.; Lucero, E.; Neeley, M.; O'connell, A.D.; Sank, D.; Wenner, J.; Martinis, J.M.; et al. Synthesizing arbitrary quantum states in a superconducting resonator. *Nature* **2009**, *459*, 546. [CrossRef] [PubMed]
12. O'Connell, A.D.; Hofheinz, M.; Ansmann, M.; Bialczak, R.C.; Lenander, M.; Lucero, E.; Neeley, M.; Sank, D.; Wang, H.; Weides, M.; et al. Quantum ground state and single-phonon control of a mechanical resonator. *Nature* **2010**, *464*, 697–703. [CrossRef] [PubMed]
13. Reiter, D.E.; Wigger, D.; Axt, V.M.; Kuhn, T. Generation and dynamics of phononic cat states after optical excitation of a quantum dot. *Phys. Rev. B* **2011**, *84*, 195327. [CrossRef]

14. Satzinger, K.J.; Zhong, Y.P.; Chang, H.S.; Peairs, G.A.; Bienfait, A.; Chou, M.H.; Cleland, A.Y.; Conner, C.R.; Dumur, É.; Grebel, J.; et al. Quantum control of surface acoustic-wave phonons. *Nature* **2018**, *563*, 661–665. [CrossRef]
15. Mahan, G.D. *Many-Particle Physics*; Plenum Press: New York, NY, USA, 1981.
16. Zrenner, A.; Beham, E.; Stufler, S.; Findeis, F.; Bichler, M.; Abstreiter, G. Coherent properties of a two-level system based on a quantum-dot photodiode. *Nature* **2002**, *418*, 612. [CrossRef]
17. Aharonovich, I.; Castelletto, S.; Simpson, D.A.; Su, C.H.; Greentree, A.D.; Prawer, S. Diamond-based single-photon emitters. *Prog. Phys.* **2011**, *74*, 076501. [CrossRef]
18. Wigger, D.; Karakhanyan, V.; Schneider, C.; Kamp, M.; Höfling, S.; Machnikowski, P.; Kuhn, T.; Kasprzak, J. Acoustic phonon sideband dynamics during polaron formation in a single quantum dot. *Opt. Lett.* **2020**, *45*, 919–922. [CrossRef] [PubMed]
19. Roca, E.; Trallero-Giner, C.; Cardona, M. Polar optical vibrational modes in quantum dots. *Phys. Rev. B* **1994**, *49*, 13704. [CrossRef] [PubMed]
20. Gali, A.; Simon, T.; Lowther, J.E. An ab initio study of local vibration modes of the nitrogen-vacancy center in diamond. *New J. Phys.* **2011**, *13*, 025016. [CrossRef]
21. Debald, S.; Brandes, T.; Kramer, B. Control of dephasing and phonon emission in coupled quantum dots. *Phys. Rev. B* **2002**, *66*, 041301. [CrossRef]
22. Munsch, M.; Kuhlmann, A.V.; Cadeddu, D.; Gérard, J.M.; Claudon, J.; Poggio, M.; Warburton, R.J. Resonant driving of a single photon emitter embedded in a mechanical oscillator. *Nat. Commun.* **2017**, *8*, 76. [CrossRef]
23. Ferry, D.K. *Semiconductors*; Macmillan: New York, NY, USA, 1991.
24. Munn, R.W.; Silbey, R. Theory of exciton transport with quadratic exciton–phonon coupling. *J. Chem. Phys.* **1978**, *68*, 2439–2450. [CrossRef]
25. Muljarov, E.A.; Zimmermann, R. Dephasing in quantum dots: Quadratic coupling to acoustic phonons. *Phys. Rev. Lett.* **2004**, *93*, 237401. [CrossRef]
26. Machnikowski, P. Change of decoherence scenario and appearance of localization due to reservoir anharmonicity. *Phys. Rev. Lett.* **2006**, *96*, 140405. [CrossRef]
27. Chenu, A.; Shiau, S.Y.; Combescot, M. Two-level system coupled to phonons: Full analytical solution. *Phys. Rev. B* **2019**, *99*, 014302. [CrossRef]
28. Duke, C.B.; Mahan, G.D. Phonon-broadened impurity spectra. I. Density of states. *Phys. Rev.* **1965**, *139*, A1965. [CrossRef]
29. Stock, E.; Dachner, M.R.; Warming, T.; Schliwa, A.; Lochmann, A.; Hoffmann, A.; Toropov, A.I.; Bakarov, A.K.; Derebezov, I.A.; Richter, M.; et al. Acoustic and optical phonon scattering in a single In (Ga) As quantum dot. *Phys. Rev. B* **2011**, *83*, 041304. [CrossRef]
30. Wigger, D.; Schneider, C.; Gerhardt, S.; Kamp, M.; Höfling, S.; Kuhn, T.; Kasprzak, J. Rabi oscillations of a quantum dot exciton coupled to acoustic phonons: Coherence and population readout. *Optica* **2018**, *5*, 1442–1450. [CrossRef]
31. Ramsay, A.J.; Godden, T.M.; Boyle, S.J.; Gauger, E.M.; Nazir, A.; Lovett, B.W.; Fox, A.M.; Skolnick, M.S. Phonon-induced Rabi-frequency renormalization of optically driven single InGaAs/GaAs quantum dots. *Phys. Rev. Lett.* **2010**, *105*, 177402. [CrossRef]
32. Hahn, T.; Groll, D.; Kuhn, T.; Wigger, D. Influence of excited state decay and dephasing on phonon quantum state preparation. *Phys. Rev. B* **2019**, *100*, 024306. [CrossRef]
33. Auffeves, A.; Richard, M. Optical driving of macroscopic mechanical motion by a single two-level system. *Phys. Rev. A* **2014**, *90*, 023818. [CrossRef]
34. Schleich, W.P. *Quantum Optics in Phase Space*; John Wiley & Sons: Berlin, Germany, 2011.
35. Gerry, C.; Knight, P.L. *Introductory Quantum Optics*; Cambridge University Press: Cambridge, UK, 2005.
36. Von Neumann, J. *Mathematische Grundlagen der Quantenmechanik*; Springer: Berlin, Germany, 1996; Volume 2.
37. Wehrl, A. General properties of entropy. *Rev. Mod. Phys.* **1978**, *50*, 221. [CrossRef]
38. Manfredi, G.; Feix, M.R. Entropy and Wigner functions. *Phys. Rev. E* **2000**, *62*, 4665. [CrossRef]
39. Brune, M.; Haroche, S.; Raimond, J.M.; Davidovich, L.; Zagury, N. Manipulation of photons in a cavity by dispersive atom-field coupling: Quantum-nondemolition measurements and generation of "Schrödinger cat"states. *Phys. Rev. A* **1992**, *45*, 5193. [CrossRef]

40. Ourjoumtsev, A.; Jeong, H.; Tualle-Brouri, R.; Grangier, P. Generation of optical 'Schrödinger cats' from photon number states. *Nature* **2007**, *448*, 784–786. [CrossRef]
41. Deleglise, S.; Dotsenko, I.; Sayrin, C.; Bernu, J.; Brune, M.; Raimond, J.M.; Haroche, S. Reconstruction of non-classical cavity field states with snapshots of their decoherence. *Nature* **2008**, *455*, 510. [CrossRef] [PubMed]